NANO LETTERS

2007
Vol. 7, No. 3
847−852

Synthesis of Colloidal Upconverting $NaYF_4$: Er^{3+}/Yb^{3+} and Tm^{3+}/Yb^{3+} Monodisperse Nanocrystals

John-Christopher Boyer, Louis A. Cuccia, and John A. Capobianco*

Department of Chemistry and Biochemistry, Concordia University, 7141 Sherbrooke Street West, Montreal, Quebec H4B 1R6, Canada

Received January 29, 2007

ABSTRACT

The synthesis, characterization, and spectroscopy of upconverting lanthanide-doped $NaYF_4$ nanocrystals (NCs) is presented. The monodisperse cubic $NaYF_4$ NCs were synthesized via a thermal decomposition reaction of trifluoroacetate precusors in a mixture of technical grade chemicals, octadecene and the coordinating ligand oleic acid. In this straightforward method, the dissolved precursors are added slowly to the reaction solution through a stainless-steel canula resulting in highly luminescent nanocrystals with an almost monodisperse particle size distribution. The NCs were characterized through the use of transmission electron microscopy, selected area electron diffraction, ^1H NMR, powder X-ray diffraction, and high-resolution luminescence spectroscopy. The $NaYF_4$ NCs are capable of being of dispersed in nonpolar organic solvents thus forming colloidally stable solutions. The colloids of the Er^{3+}, Yb^{3+} and Tm^{3+}, Yb^{3+} doped NCs exhibit green/red and blue upconversion luminescence, respectively, under 980 nm laser diode excitation with low power densities.

The synthesis and spectroscopy of upconverting nanocrystals (NCs) has garnered a tremendous amount of attention in the literature recently.[1−9] Upconversion is a process where low-energy light, usually near-infrared (NIR) or infrared (IR), is converted to higher energies, ultraviolet (UV) or visible, via multiple absorptions or energy transfers.[10,11] This phenomenon has been observed in transition metal, lanthanide, and actinide ions, though the highest efficiencies are found in lanthanide-doped materials. To date, the highest upconversion efficiencies observed have been in hexagonal phase $NaYF_4$ bulk materials doped with the Er^{3+}/Yb^{3+} or Tm^{3+}/Yb^{3+} ion couples synthesized via solid-state methods.[12,13] Colloids of upconverting $NaYF_4$ NCs, and the related material $NaGdF_4$, have also been synthesized through thermal decomposition, precipitation, and high-pressure reactions.[1,5,7,8,14] The ability to suspend upconverting NCs as clear colloidal solutions has opened the door for their use in several new technologies, the most promising of which appears to be for use as labels in biological assays and imaging.

Upconverting $NaYF_4$ NCs doped with the Er^{3+}/Yb^{3+} have already been successfully applied to analyte and DNA detection.[6, 9] The use of upconverting nanophosphors for bioimaging has also been demonstrated.[15] The majority of current commercialized labels, such as organic dyes and quantum dots (QDs), utilize the Stokes luminescence of the fluorophore under UV, blue, or green excitation in order to detect the analyte. This leads to the possibility of high background signals and difficulty in choosing an appropriate label as many biological species fluoresce under ultraviolet or visible radiation. The use of upconverting NCs, two-photon dyes or two-photon QDs removes many of these difficulties.[16−24] The drawback with the use of dyes or quantum dots is the need for expensive pulse lasers to meet the high power densities required to observe the two-photon effect.[16,17,24] One may also increase the sensitivity further by choosing a detection system with low response in the wavelength range of the IR excitation source.

We have previously synthesized upconverting cubic $NaYF_4$ NCs doped with the Er^{3+}/Yb^{3+} or Tm^{3+}/Yb^{3+} ion couples via the thermal decomposition of trifluoroacetate precursors in a high-boiling point organic sovent.[25] A similar approach was used in the literature to produce sodium rare-earth fluoride nanocrystals and LaF_3 nanoplates.[8,26] These procedures take advantage of the fact that the metal trifluoroacetates thermally decompose to give the corresponding metal fluorides at relatively low temperatures (200−300 °C).[27−30] In these methods the noncordinating solvent octadecene was used as the primary solvent due to its high boiling point (315 °C). Oleic acid was chosen as the coordinating ligand due to its successful use in the synthesis of various types of nanocrystals.[31,32]

In this paper we present a modification to our previously reported synthetic procedure for upconverting, cubic $NaYF_4$ particles doped with either Er^{3+}/Yb^{3+} or Tm^{3+}/Yb^{3+}. Though

* Corresponding author: tel, +1-514-848-2424 ext. 3350; fax, +1-515-848-2868; e-mail, capo@vax2.concordia.ca.

10.1021/nl070235+ CCC: $37.00
Published on Web 02/16/2007

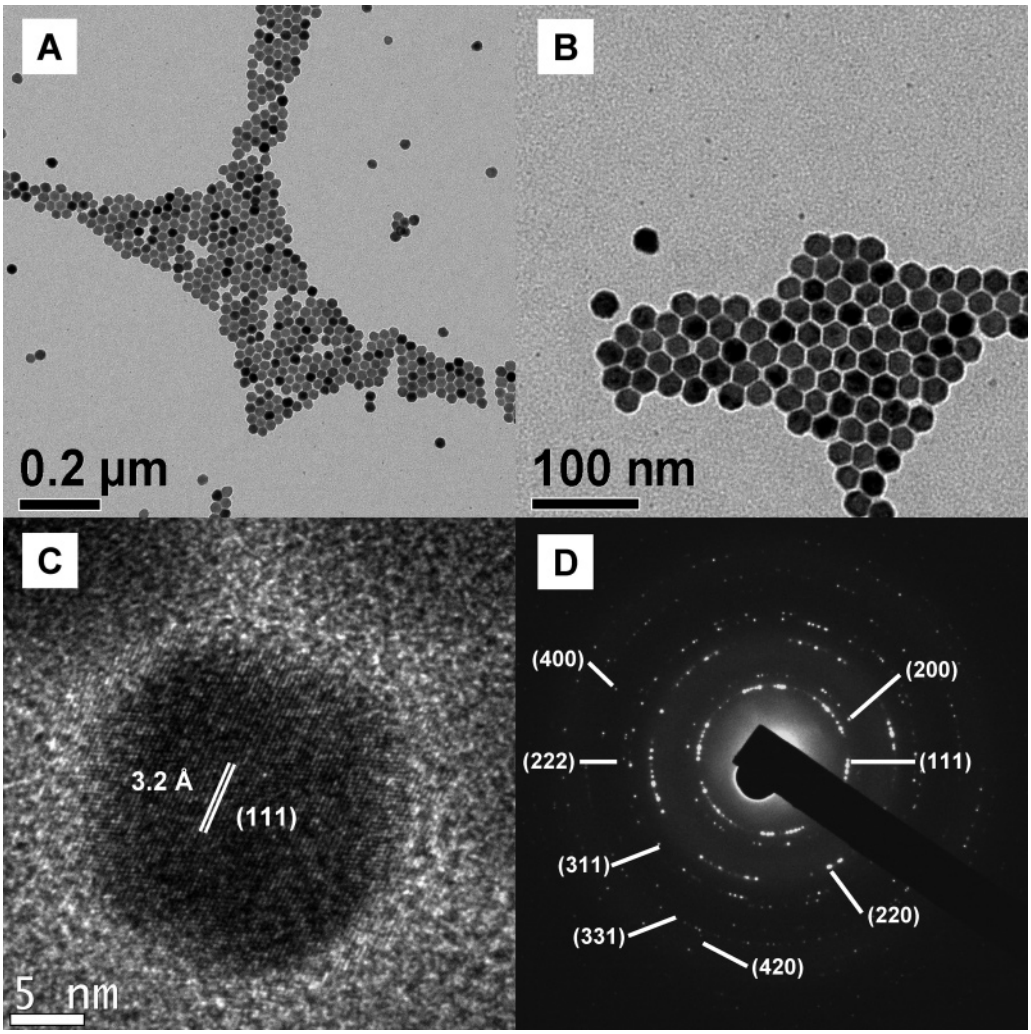

Figure 1. (A, B) Low-resolution transmission electron micrographs of $NaYF_4$: 2% Er^{3+}, 20% Yb^{3+} sample showing uniformity of the particles. (C) High-resolution micrographs of a single $NaYF_4$: 2% Er^{3+}, 20% Yb^{3+} particle showing lattice fringes. (D) Selected area electron diffraction pattern (SAED) of $NaYF_4$: 2% Er^{3+}, 20% Yb^{3+} particles.

our previously reported synthetic procedure was a significant advancement in the synthesis of upconverting nanoparticles, refinement of the synthesis was still required to obtain nanoparticles with a defined shape and a narrower particle size range. Our previous synthesis resulted in particles with nonuniform shape and a wide particle size range (10−60 nm). By introducing the lanthanide precursors slowly into the high-temperature reaction mixture through a stainless-steel canula, we were able to synthesize nanoparticles with a regular shape and a monodisperse particle size distribution. These particles are capable of being colloidally dispersed in various nonpolar organic solvents (e.g., hexane, toluene, dichloromethane) and are able to emit visible light under 980 nm laser diode excitation via the upconversion process under relatively low excitation power densities. This method uses inexpensive technical grade chemicals which reduces the cost of the nanoparticle synthesis and a relatively low cost laser diode for excitation hence making them attractive for potential commercial applications.

The synthesis report here for $NaYF_4$ NCs is a modification of recently reported synthetic procedures for LaF_3 nanoplates and $NaYF_4$ NCs.[8,25,26] The lanthanide trifluoroacetate precursors for the synthesis were prepared from the corresponding lanthanide oxides and trifluoroacetic acid in a three-neck round-bottom flask. The corresponding amount of sodium trifluoroacetate was then added to the lanthanide trifluoroacetates in the reaction vessel with 5 mL of octadecene and 10 mL of oleic acid. A second solution of 15 mL of octadecene and 10 mL oleic acid was then prepared in a second three-neck round-bottom flask. Both solutions were heated slowly to 125 °C under vacuum with stirring and kept at this temperature for 30 min to remove residual water and oxygen. The second solution was then heated to 310 °C under argon and maintained at this temperature. The lanthanide trifluoroacetate solution at 125 °C was then transferred dropwise into the second solution over a period of 15 min using a stainless steel cannula at a flow rate of ca. 1 mL/min. During this time the second solution was maintained at 310 °C. After the addition was complete the temperature of the reaction mixture was lowered to 305 °C and kept at this temperature for 1 h under dry argon. Subsequently the mixture was removed from the heating mantle and cooled to room temperature. The NCs were precipitated by the addition of excess ethanol and isolated via centrifugation.

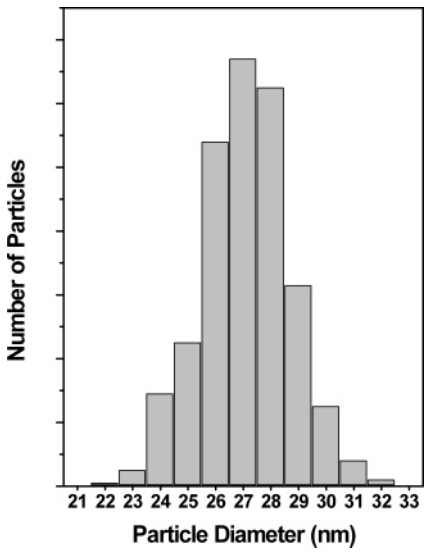

Figure 2. Histogram of the particle sizes obtained from TEM images of ~500 $NaYF_4$: 2% Er^{3+}, 20% Yb^{3+} nanocrystals (average particle size = 27.6 ± 1.6 nm).

The resulting pellet was then washed twice by dispersing with ethanol and centrifugated. The resulting NCs were dried under air for 24 h. Due to the presence of the capping ligand, the NCs could be dispersed in nonpolar solvents and were colloidally stable in solution for a period of weeks with no visible agglomeration or settling. A more detailed description of the synthetic procedure and spectroscopy setup is given in the Supporting Information of the article.

Figure 1 shows the transmission electron microscopy (TEM) data for a $NaYF_4$: 2% Er^{3+}, 20% Yb^{3+} NC sample. From the low-resolution micrographs, panels A and B of Figure 1, one can observe that the synthesized particles appear hexagonal in shape and are nearly monodisperse. From a detailed particle size analysis of 500 particles from several low-resolution TEM micrographs (Figure 2), the average particle size was found to be 27.6 nm with a standard deviation of 1.6 nm. Further proof of the uniform particle size and shape of the particles reported herein is provided by their assembly into a regular two-dimensional hexagonal close packed arrangement on the TEM grid due to the presence of the oleic acid capping ligand on the surface of the particles.

From the high-resolution TEM (HRTEM) image, Figure 1C, the distance between the particles was found to be 2.8 ± 0.5 nm which is somewhat less than two times the length of a single oleate molecule (2.2 nm from semiempirical calculation). This is a good indication that there is interdigitation of the alkyl chains from neighboring particles or that the oleic acid chains are not in a fully extended conformation. From the HRTEM image one can also clearly distinguish lattice fringes on the individual particles indicating that the particles are highly crystalline. The distances between the lattice fringes were measured to be 3.2 and 2.8 which correspond to the *d*-spacing for the (111) and (200) lattice planes, respectively, in the cubic $NaYF_4$ structure.[33−35] From this we can conclude that the particles have a polyhedron shape and are truncated octahedrons bordered by the (111) and (002) lattice planes.[36] The hexagonal shape of the particles observed in the TEM images are two-dimensional projections of the three-dimensional truncated octahedral geometry. The selected area electron diffraction (SAED) pattern of the particles (Figure 1D) can be indexed to the (111), (200), (220), (311), (222), (400), and (331) planes of the standard cubic α-$NaYF_4$ structure (JCPDS: 6-0342) as seen in Table 1. As well, the particles were found to be single crystallites as the Fourier transformation on individual particles returned patterns corresponding to a single set of (111) and (200) planes.

In a previous study we found that the synthesis of α-$NaYF_4$ nanoparticles in octadecene and oleic acid resulted in irregularly shaped particles with a wide particle size range.[25] It is clear from the TEM data that the modifications made to the earlier synthetic procedure result in α-$NaYF_4$ nanoparticles with a defined shape and monodisperse size distribution. It can be assumed that the decomposition of the trifluoroacetate precursors and thus the crystallization of the $NaYF_4$ particles occur quite fast at the temperatures used in this synthesis (310 °C). By adding the precursors to the solution slowly, one can control the rate of decomposition and formation of the particles. In essence, by performing the addition over a longer period of time one can separate the nucleation and growth phases of the nanocrystals resulting in a monodisperse particle size. This method also allows the oleic acid to complex to the surface of the growing particles more effectively due to the initial low concentration of precursor in the solution. The oleic acid ligands modulates the growth rate along the ⟨111⟩ and ⟨200⟩ directions of the cubic $NaYF_4$ nanocrystals resulting in the truncated octahedral shape.

The presence of the oleic acid ligand on the surface of the NCs was confirmed using ^{1}H NMR of an undoped $NaYF_4$ sample. The ^{1}H NMR of the undoped $NaYF_4$ sample dispersed in $CDCl_3$ is shown in Figure S1 in Supporting Information, along with the ^{1}H NMR of free oleic acid for reference. The ^{1}H NMR signals of the bound oleic acid molecules on the surface of the nanoparticles are broadened with respect to those of the free oleic acid. The broadening is due to an inhomogeneous distribution of the magnetic environments due to site variations on the nanoparticle surface as well as a decrease in the rotational freedom of the oleic acid ligands.[37−39]

Figure 3 shows the powder X-ray diffraction (XRD) patterns for the $NaYF_4$: 2% Er^{3+}, 20% Yb^{3+}; $NaYF_4$: 2% Tm^{3+}, 20% Yb^{3+}; and $NaYF_4$ NCs, as well as the calculated line pattern for α-$NaYF_4$. It is evident from the intensity of the peaks in the obtained patterns that the materials in question are highly crystalline in nature. The peak positions of all three patterns correspond closely to the reported and calculated patterns for cubic α-$NaYF_4$.[33−35] The calculated *d* spacing values for all three samples and the corresponding *h k l* values are given in Table 1. These values obtained from the nanocrystalline samples closely match the standard pattern of α-$NaYF_4$ (JCPDS: 6-0342), and no peaks from other phases or impurities were observed. The lattice constants for the $NaYF_4$: 2% Er^{3+}, 20% Yb^{3+}; $NaYF_4$: 2%

Table 1. *d*-Spacing Values for $NaYF_4$: 2% Er^{3+}, 20% Yb^{3+}; $NaYF_4$: 2% Tm^{3+}, 20% Yb^{3+}; and $NaYF_4$ Determined via Electron Diffraction (ED) and X-ray Diffraction (XRD)

	d-spacing values (Å)				
h k l	$NaYF_4$: 2% Er^{3+}, 20% Yb^{3+} (ED)	$NaYF_4$: 2% Er^{3+}, 20% Yb^{3+} (XRD)	$NaYF_4$: 2% Tm^{3+}, 20% Yb^{3+} (XRD)	$NaYF_4$ (XRD)	standard pattern (JCPDS: 6-0342)
1 1 1	3.15	3.19	3.19	3.19	3.14
2 0 0	2.72	2.76	2.76	2.76	2.73
2 2 0	1.92	1.95	1.95	1.95	1.93
3 1 1	1.64	1.66	1.66	1.66	1.64
2 2 2	1.57	1.59	1.59	1.59	1.57
4 0 0	1.36	1.38	1.38	1.38	1.36
3 3 1	1.26	1.27	1.27	1.26	1.25
4 2 0	1.22	1.23	1.23	1.23	1.22

Tm^{3+}, 20% Yb^{3+}; and $NaYF_4$ NCs were calculated to be 5.519, 5.515, and 5.517 Å, respectively, which correspond closely to previously reported lattice constants of 5.485 and 5.47 Å for nanocrystalline[1] and bulk α-$NaYF_4$.[35] The broad nature of the observed diffraction peaks is an indication of the small size of the NCs. From the line broadening of the (111) diffraction peak of the $NaYF_4$: 2% Er^{3+}, 20% Yb^{3+} sample, an average crystallite size of 25 nm was calculated using the Debye−Sherrer formula. This value matches closely to the particle size determined from the TEM results.

The upconversion spectra of both 1 wt % solutions of $NaYF_4$: 2% Er^{3+}, 20% Yb^{3+} and $NaYF_4$: 2% Tm^{3+}, 20% Yb^{3+} nanocrystals in toluene under 980 nm laser diode excitation (power density = 100 W/cm^2) are shown in parts A and B of Figure 4, respectively, and correspond to what has been reported previously for these materials.[1, 25] The emission bands can easily be assigned to transitions within the 4f−4f levels of the Er^{3+} and Tm^{3+} ions. The spectrum of the $NaYF_4$: 2% Er^{3+}, 20% Yb^{3+} sample (Figure 4A) exhibits three distinct Er^{3+} emission bands. The green emissions between 510 and 530 nm and between 530 and 570 nm were assigned to the $^2H_{11/2} \rightarrow {}^4I_{15/2}$ and $^4S_{3/2} \rightarrow {}^4I_{15/2}$ transitions, respectively. A dominant red emission was observed between 635 and 700 nm originating from the $^4F_{9/2} \rightarrow {}^4I_{15/2}$ transition as well as a weak NIR emission between 830 and 860 nm corresponding to the $^4S_{3/2} \rightarrow {}^4I_{13/2}$ transition. The inset of Figure 4A shows a digital photograph of the total upconversion luminescence of the same solution under the excitation conditions. The total luminescence appears yellow-green in color due to a combination of green and red emissions from the Er^{3+} ion. This is apparent in the other two digital photographs where the solution is viewed through

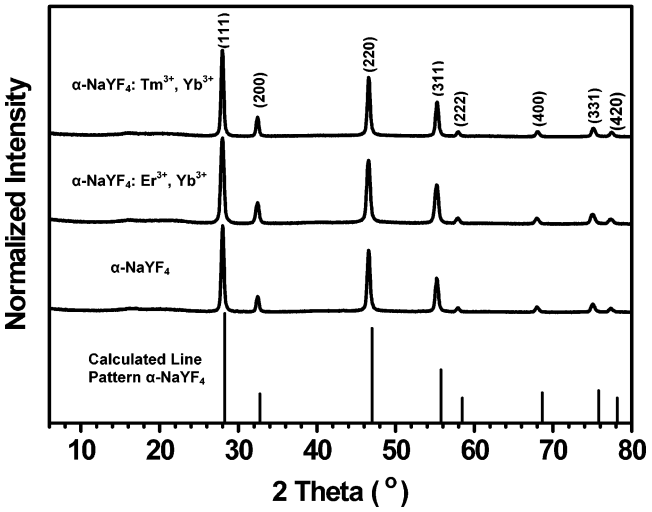

Figure 3. Experimental powder X-ray diffraction (XRD) patterns of α-$NaYF_4$, α-$NaYF_4$: 2% Er^{3+}, 20% Yb^{3+} and α-$NaYF_4$: 2% Tm^{3+}, 20% Yb^{3+}nanocrystals. Calculated line pattern for α-$NaYF_4$ (bottom plot) is shown for reference.

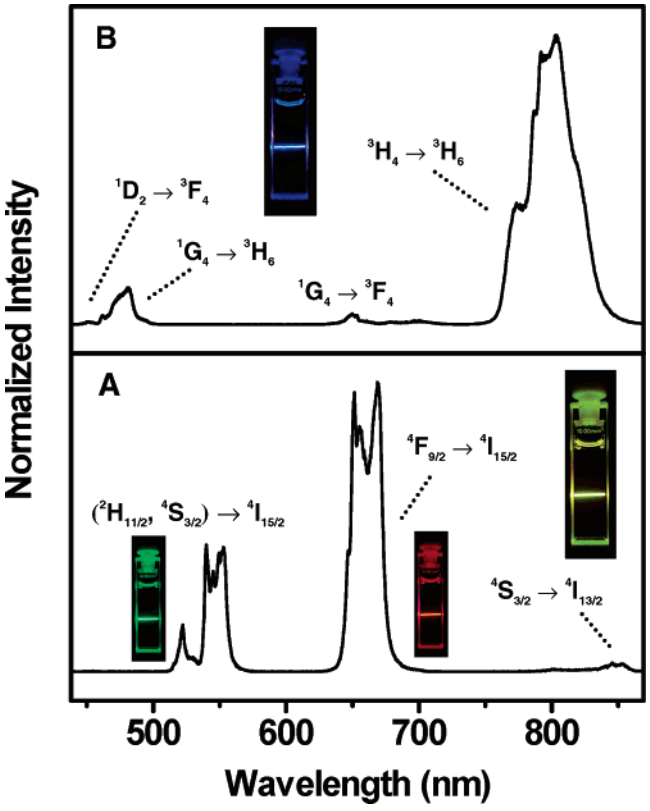

Figure 4. Luminescence emission spectra of 1 wt % colloidal solutions of nanocrystals in toluene excited with a 980 nm laser diode (power density = 100 W/cm^2): (A) $NaYF_4$: 2% Er^{3+}, 20% Yb^{3+} and (B) $NaYF_4$: 2% Tm^{3+}, 20% Yb^{3+}. (Inset A) Total upconversion luminescence of $NaYF_4$: 2% Er^{3+}, 20% Yb^{3+} solution and isolation of green and red luminescence using appropriate filters. (Inset B) Total upconversion luminescence of $NaYF_4$: 2% Tm^{3+}, 20% Yb^{3+} solution. Adapted from Figures 2 and 3 of ref 25.

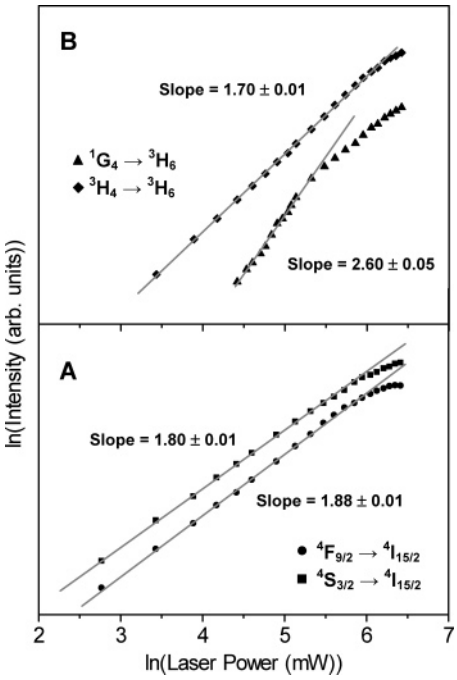

Figure 5. Power dependence of the upconverted emissions of 1 wt % colloidal solutions of nanocrystals in toluene excited at 980 nm: (A) $NaYF_4$: 2% Er^{3+}, 20% Yb^{3+} and (B) $NaYF_4$: 2% Tm^{3+}, 20% Yb^{3+}. The straight lines are least-squares fits to the low power data points as at higher excitation densities the power dependence of the emissions are observed to level off due to saturation of the upconversion processes.

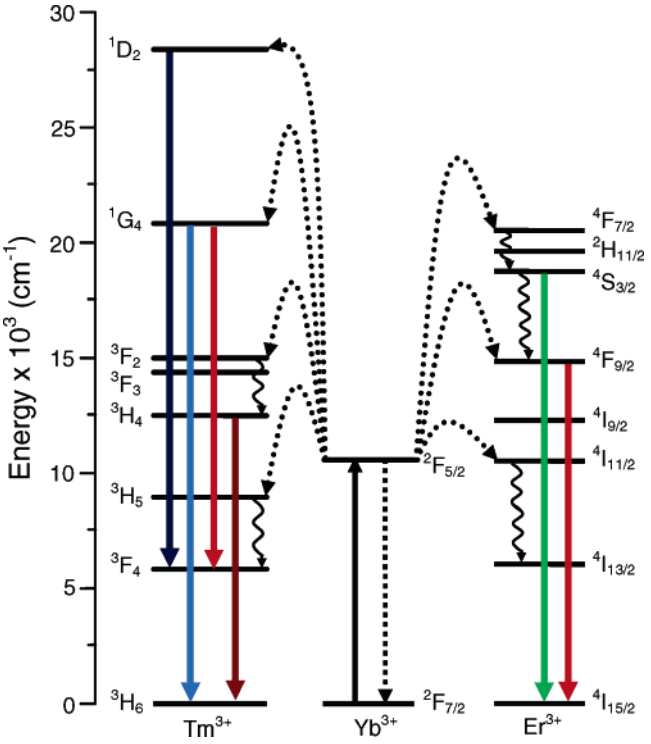

Figure 6. The energy level diagrams of the Er^{3+}, Tm^{3+}, and Yb^{3+} dopant ions and upconversion mechanisms following 980 nm laser diode excitation. The full, dotted, and curly arrows represent emission, energy transfer, and multiphonon relaxation processes, respectively.

green and red filters, respectively, thus isolating the two separate emissions.

Four Tm^{3+} emission bands were observed in the $NaYF_4$: 2% Tm^{3+}, 20% Yb^{3+} sample (Figure 4B) upon 980 nm laser diode excitation. The band observed in the blue region of the spectrum between 440 and 500 nm was assigned to the $^1D_2 \rightarrow {}^3F_4$ and $^1G_4 \rightarrow {}^3H_6$ transitions. A week red emission between 630 and 670 nm and an intense NIR emission between 750 and 850 nm were assigned to the $^1G_4 \rightarrow {}^3F_4$ and $^3H_4 \rightarrow {}^3H_6$ transitions, respectively. The inset of Figure 4B shows a digital photograph of the 1 wt % solution of $NaYF_4$: 2% Tm^{3+}, 20% Yb^{3+} NCs under the excitation conditions.

In order to determine the number of photons responsible for the upconversion mechanism, the intensities of the upconversion emissions were recorded as a function of the 980 nm excitation intensity (Figure 5). As seen in Figure 5A, the green and red Er^{3+} upconversion emission intensities demonstrated quadratic power dependencies at low excitation densities indicating two photon upconversion mechanisms. For the Tm^{3+}-doped sample (Figure 5B), three and two photon power dependencies were observed for the $^1G_4 \rightarrow {}^3H_6$ and $^3H_4 \rightarrow {}^3H_6$ emissions at low excitation densities, respectively. The power dependencies of the Er^{3+} and Tm^{3+} upconversion emissions became linear at high excitation densities due to "saturation" of the upconversion processes.[40] Upconversion is a nonlinear process; as such it will not maintain its nonlinear behavior up to infinite excitation energies as a consequence of the conservation of energy. Hence at high excitation densities, the power dependence of the upconversion luminescence intensity will become linear, and a "saturation" of the luminescence intensity is observed.

The upconversion excitation pathways for the Er^{3+}/Yb^{3+} and Tm^{3+}/Yb^{3+} ion couples in these materials are well-known[41] and are shown in Figure 6. In the case of $NaYF_4$: 2% Er^{3+}, 20% Yb^{3+}, an initial energy transfer from an Yb^{3+} ion in the $^2F_{5/2}$ state to an Er^{3+} ion populates the $^4I_{11/2}$ level. A second 980 nm photon, or energy transfer from an Yb^{3+} ion, can then populate the $^4F_{7/2}$ level of the Er^{3+} ion. The Er^{3+} ion can then relax nonradiatively (without emission of photons) to the $^2H_{11/2}$ and $^4S_{3/2}$ levels, and the green $^2H_{11/2} \rightarrow {}^4I_{15/2}$ and $^4S_{3/2} \rightarrow {}^4I_{15/2}$ emissions occur. Alternatively, the ion can further relax and populate the $^4F_{9/2}$ level leading to the red $^4F_{9/2} \rightarrow {}^4I_{15/2}$ emission. The $^4F_{9/2}$ level may also be populated from the $^4I_{13/2}$ level of the Er^{3+} ion by absorption of a 980 nm photon, or energy transfer from an Yb^{3+} ion, with the $^4I_{13/2}$ state being initially populated via the nonradiative $^4I_{11/2} \rightarrow {}^4I_{13/2}$ relaxation. For the $NaYF_4$: 2% Tm^{3+}, 20% Yb^{3+} sample, up to four subsequent energy transfers from Yb^{3+} ions populate the upper Tm^{3+} levels (Figure 6) and the various emissions can occur.

In summary, we have prepared upconverting lanthanide-doped $NaYF_4$ nanocrystals (NCs) from the thermal decomposition reaction of trifluoroacetate precursors in a mixture of octadecene and oleic acid. The nanocrystals produced by this method are ~28 nm in diameter on average with an almost monodisperse particle size distribution. SAED and powder XRD indicate the nanocrystals are cubic α-$NaYF_4$.

HRTEM shows that the nanocrystals are highly crystalline and are composed of single crystallites. The Er^{3+}/Yb^{3+} and Tm^{3+}/Yb^{3+} doped nanocrystals are capable of upconverting NIR light from a 980 nm diode laser into red/green and blue light, respectively.

The synthetic method presented here is highly attractive as it uses technical grade solvents and ligands and yet produces highly luminescent and uniform NCs. The synthesis does not require sophisticated equipment or complicated procedures, and the resulting NCs are capable of being excited with a 980 nm laser diode thereby increasing their commercialization possibilities. Upconverting NCs have already been identified for potential use as biolabels and in biological assays. Further research is currently underway to modify the oleic acid-capped surface to obtain water-soluble particles required for these applications.

Acknowledgment. The authors gratefully acknowledge the Natural Sciences and Engineering Research Council (NSERC) of Canada for financial support.

Supporting Information Available: Full synthetic and experimental procedure and NMR of $NaYF_4$ sample and free oleic acid. This material is available free of charge via the Internet at http:// pubs.acs.org.

References

(1) Heer, S.; Kömpe, K.; Güdel, H. U.; Haase, M. *Adv. Mater.* **2004**, *16* (23−24), 2102−2105.
(2) Lu, H.; Yi, G.; Zhao, S.; Chen, D.; Guo, L.-H.; Cheng, J. *J. Mater. Chem.* **2004**, *14* (8), 1336−1341.
(3) Yi, G.; Lu, H.; Zhao, S.; Ge, Y.; Yang, W.; Chen, D.; Guo, L.-H. *Nano Lett.* **2004**, *4* (11), 2191−2196.
(4) Sivakumar, S.; Veggel, F. C. J. M. V.; Raudsepp, M. *J. Am. Chem. Soc.* **2005**, *127* (36), 12464−12465.
(5) Suyver, J. F.; Aebischer, A.; Biner, D.; Gerner, P.; Grimm, J.; Heer, S.; Krämer, K. W.; Reinhard, C.; Güdel, H. U. *Opt. Mater.* **2005**, *27* (6), 1111−1130.
(6) Wang, L.; Yan, R.; Huo, Z.; Wang, L.; Zeng, J.; Bao, J.; Wang, X.; Peng, Q.; Li, Y. *Angew. Chem., Int. Ed.* **2005**, *44* (37), 6054−6057.
(7) Zeng, J.-H.; Su, J.; Li, Z.-H.; Yan, R.-X.; Li, Y.-D. *Adv. Mater.* **2005**, *17* (17), 2119−2123.
(8) Mai, H.-X.; Zhang, Y.-W.; Si, R.; Yan, Z.-G.; Sun, L.; You, L.-P.; Yan, C.-H. *J. Am. Chem. Soc.* **2006**, *128* (19), 6426−6436.
(9) Wang, L.; Li, Y. *Chem. Commun.* **2006**, *24*, 2557−2559.
(10) Scheps, R. *Prog. Quantum Electron.* **1996**, *20* (4), 271−358.
(11) Auzel, F. *Chem. Rev.* **2004**, *104* (1), 139−173.
(12) Krämer, K. W.; Biner, D.; Frei, G.; Güdel, H. U.; Hehlen, M. P.; Lüthi, S. R. *Chem. Mater.* **2004**, *16* (7), 1244−1251.
(13) Suyver, J. F.; Grimm, J.; Krämer, K. W.; Güdel, H. U. *J. Lumin.* **2005**, *114* (1), 53−59.
(14) Aebischer, A.; Heer, S.; Biner, D.; Krämer, K.; Haase, M.; Güdel, H. U. *Chem. Phys. Lett.* **2005**, *407* (1−3), 124−128.
(15) Lim, S. F.; Riehn, R.; Ryu, W. S.; Khanarian, N.; Tung, C.-K.; Tank, D.; Austin, R. H. *Nano Lett.* **2006**, *6* (2), 169−174.
(16) König, K. *J. Microsc.* **2000**, *200* (2), 83−104.
(17) Larson, D. R.; Zipfel, W. R.; Williams, R. M.; Clark, S. W.; Bruchez, M. P.; Wise, F. W.; Webb, W. W. *Science* **2003**, *300* (5624), 1434−1437.
(18) Kuningas, K.; Rantanen, T.; Ukonaho, T.; Lövgren, T.; Soukka, T. *Anal. Chem.* **2005**, *77* (22), 7348−7355.
(19) Hirai, T.; Orikoshi, T. *J. Colloid Interface Sci.* **2004**, *273* (2), 470−477.
(20) Hampl, J.; Hall, M.; Mufti, N. A.; Yao, Y.-M. M.; MacQueen, D. B.; Wright, W. H.; Cooper, D. E. *Anal. Biochem.* **2001**, *288* (2), 176−187.
(21) Corstjens, P. L. A. M.; Li, S.; Zuiderwijk, M.; Kardos, K.; Abrams, W. R.; Niedbala, R. S.; Tanke, H. J. *IEEE Proc., Nanobiotechnol.* **2005**, *152* (2), 64−72.
(22) Niedbala, R. S.; Feindt, H.; Kardos, K.; Vail, T.; Burton, J.; Bielska, B.; Li, S.; Milunic, D.; Bourdelle, P.; Vallejo, R. *Anal. Biochem.* **2001**, *293* (1), 22−30.
(23) Rijke, F. v. d.; Zijlmans, H.; Li, S.; Vail, T.; Raap, A. K.; Niedbala, R. S.; Tanke, H. J. *Nat. Biotechnol.* **2001**, *19* (3), 273−276.
(24) Denk, W.; Strickler, J. H.; Webb, W. W. *Science* **1990**, *248* (4951), 73−76.
(25) Boyer, J.-C.; Vetrone, F.; Cuccia, L. A.; Capobianco, J. A. *J. Am. Chem. Soc.* **2006**, *128* (23), 7444−7445.
(26) Zhang, Y.-W.; Sun, X.; Si, R.; You, L.-P.; Yan, C.-H. *J. Am. Chem. Soc.* **2005**, *127* (10), 3260−3261.
(27) Rüssel, C. *J. Mater. Sci. Lett.* **1992**, *11* (3), 152−154.
(28) Rüssel, C. *J. Non-Cryst. Solids* **1993**, *152* (2−3), 161−166.
(29) Wagener, U.; Rüssel, C. *J. Non-Cryst. Solids* **1993**, *152* (2−3), 167−171.
(30) Rillings, K. W.; Roberts, J. E. *Thermochim. Acta* **1974**, *10* (3), 285−*98.*
(31) Park, J.; An, K.; Hwang, Y.; Park, J.-G.; Noh, H.-J.; Kim, J.-Y.; Park, J.-H.; Hwang, N.-M.; Hyeon, T. *Nat. Mater.* **2004**, *3* (12), 891−895.
(32) Yu, W. W.; Peng, X. *Angew. Chem., Int. Ed.* **2002**, *41* (13), 2368−2371.
(33) Pol, P. G.; Rao, V. J. *Indian J. Pure Appl. Phys.* **1973**, *11* (12), 886−8.
(34) Reddy, K.; Narasimha, S.; Shareef, M. A. H.; Pandaraiah, N. *J. Mater. Sci. Lett.* **1983**, *2* (2), 83−84.
(35) Roy, D. M.; Roy, R. *J. Electrochem. Soc.* **1964**, *111* (4), 421−429.
(36) Wang, Z. L. *J. Phys. Chem. B* **2000**, *104* (6), 1153−1175.
(37) Sudarsan, V.; Sivakumar, S.; Veggel, F. C. J. M. v. *Chem. Mater.* **2005**, *17* (18), 4736−4742.
(38) Sachleben, J. R.; Wooten, E. W.; Emsley, L.; Pines, A.; Colvin, V. L.; Alivisatos, A. P. *Chem. Phys. Lett.* **1992**, *198* (5), 431−436.
(39) Kuno, M.; Lee, J. K.; Dabbousi, B. O.; Mikulec, F. V.; Bawendi, M. G. *J. Chem. Phys.* **1997**, *23*, 9869−9882.
(40) Pollnau, M.; Gamelin, D. R.; Lüthi, S. R.; Güdel, H. U. *Phys. Rev. B* **1999**, *61* (5), 3337−3346.
(41) Page, R. H.; Schaffers, K. I.; Waide, P. A.; Tassano, J. B.; Payne, S. A.; Krupke, W. F.; Bischel, W. K. *J. Opt. Soc. Am. B* **1998**, *15* (3), 996−1008.

NL070235+